

# Brain-ID: Learning Robust Feature Representations for Brain Imaging

Peirong Liu<sup>1,\*</sup> Oula Puonti<sup>1,2</sup> Xiaoling Hu<sup>1</sup> Daniel C. Alexander<sup>3</sup> Juan Eugenio Iglesias<sup>1,3,4</sup>

<sup>1</sup>Athinoula A. Martinos Center for Biomedical Imaging,  
Massachusetts General Hospital and Harvard Medical School

<sup>2</sup>Danish Research Centre for Magnetic Resonance,  
Centre for Functional and Diagnostic Imaging and Research,  
Copenhagen University Hospital - Amager and Hvidovre

<sup>3</sup>Centre for Medical Image Computing, University College London

<sup>4</sup>Computer Science and Artificial Intelligence Laboratory, Massachusetts Institute of Technology

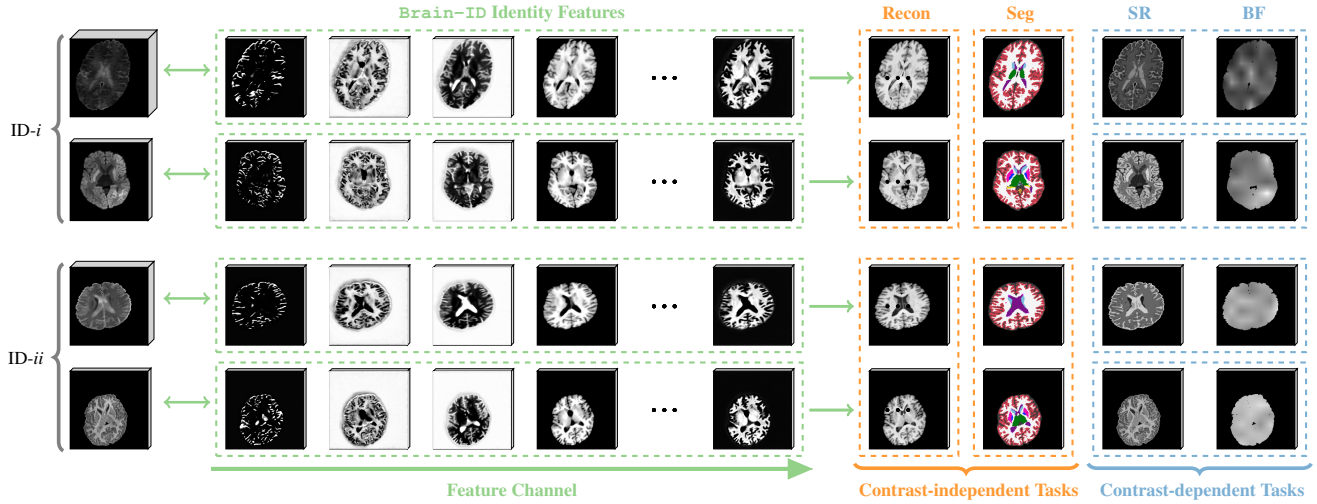


Figure 1. Brain-ID features are robust to identity (subject) regardless of its appearance (deformation, MR contrast, resolution, orientation, noise, artifacts, etc), and can be easily adapted to a series of downstream applications, including both contrast-independent tasks (anatomy **Recon**struction/contrast synthesis, brain **Seg**mentation), and contrast-dependent tasks (**SR** Super-Resolution, **BF** Bias Field estimation).

## Abstract

Recent learning-based approaches have made astonishing advances in calibrated medical imaging like computerized tomography, yet they struggle to generalize in uncalibrated modalities – notoriously magnetic resonance imaging (MRI), where performance is highly sensitive to the differences in MR contrast, resolution, and orientation between the training and testing data. This prevents broad applicability to the diverse clinical acquisition protocols in the real world. We introduce Brain-ID, a robust feature representation learning strategy for brain imaging, which is contrast-agnostic, and robust to the brain

anatomy of each subject regardless of the appearance of acquired images (i.e., deformation, contrast, resolution, orientation, artifacts, etc). Brain-ID is trained entirely on synthetic data, and easily adapts to downstream tasks with our proposed simple one-layer solution. We validate the robustness of Brain-ID features, and evaluate their performance in a variety of downstream applications, including both contrast-independent (anatomy reconstruction/contrast synthesis, brain segmentation), and contrast-dependent (super-resolution, bias field estimation) tasks (Fig. 1). Extensive experiments on 6 public datasets demonstrate that Brain-ID achieves state-of-the-art performance in all tasks, and more importantly, preserves its performance when only limited training data is available.

\* Correspondence to: pliul7@mgh.harvard.edu

## 1. Introduction

Magnetic resonance imaging (MRI) enables in vivo noninvasive imaging of the human brain with exquisite and tunable soft-tissue contrast [5]. Recent machine learning based methods have achieved great improvements in faster and more accurate image analysis of brain MRI [21], such as image segmentation [14, 25, 31, 36], registration [2, 13, 49], super-resolution [39, 40], and connectivity studies [34]. However, most existing MRI analysis methods are specific to certain MR contrast(s) and often require near-isotropic acquisitions. Therefore, models face sharp performance drops when voxel size and anisotropy increase, or are being used for a different contrast than that for training [43]. This reduces model generalizability and results in duplicate data collection and training efforts given new datasets. By resorting to synthetic data, recent contrast-agnostic models [3, 19, 21, 22] achieve impressive results and largely extend the applicability of models to heterogeneous clinical acquisition protocols. However, these models are only applicable to the task they are trained for.

Meanwhile, task-agnostic foundation models in computer vision and natural language processing have witnessed remarkable success, along with the fast developments of large-scale datasets [7, 10, 26]. Designed in a task-agnostic manner, foundation models have shown impressive performance in obtaining more general feature representations and can be quickly adapted (e.g., fine-tuned) to a wide range of downstream tasks [1, 4]. However, due to different acquisition protocols, processing pipelines, and privacy requirements across institutions, large-scale datasets in medical imaging require significantly more effort than natural imaging/language. As a result, medical foundation models are not as well developed. The MONAI<sup>1</sup> project includes a model zoo containing pre-trained models for various tasks, yet they are all highly task-oriented and sensitive to specific image contrasts. Zhou et al. [51] constructed a medical foundation model, yet it is designed for the detection of eye and systemic health conditions from retinal scans, and only works on the modalities of color fundus photography and optical coherence tomography. Lately, generalist biomedical AI systems (e.g., GMAI [33], Med-PaLM M [37, 41]), have shown great potential in biomedical tasks under vision-language context, e.g., (visual) question answering, image classification, radiology report generation and summarization. However, they have not explored more challenging vision tasks such as image reconstruction, segmentation, super-resolution, and registration.

Here we introduce Brain-ID, an identity-robust, contrast-agnostic, and task-independent feature representation strategy which is trained *entirely* on synthetic data.

- 1) We present our on-the-fly data generator which simulates

any combination of image deformation, contrast, resolution, orientation, noises, artifacts, etc, for each subject. While real-world datasets are restricted to the contrast(s) acquired per subject, our simulator exposes Brain-ID to a much richer learning space (Fig. 2).

- 2) We propose a general feature representation learning strategy guided by the *unique* anatomy of each subject. The resulting high-resolution features are robust to the superficial perturbations of the input image’s appearance (Sec. 4.2) such as contrast, resolution, orientation, artifacts, and can easily adapt to the downstream tasks with a simple one-layer modification (Sec. 3.3).
- 3) We extensively evaluate the properties of Brain-ID features on both contrast-independent (anatomy reconstruction, brain segmentation) and contrast-dependent (super-resolution, bias field estimation) tasks. We experiment on 6 public datasets (around 8,000 images in total) including different modalities of MR (T1, T2, FLAIR) and CT. Brain-ID achieves state-of-the-art performance in all tasks (Tab. 2, Fig. 5), and preserves its performance when dealing with training datasets of limited size (Fig. 6).

## 2. Related work

**Feature Representation in Medical Imaging** As discussed in Sec. 1, general feature representation learning in the medical imaging context is much more challenging than in the natural image domain, due to limited data accessibility, lack of data diversity, and being highly domain-specific. Xu et al. [47] introduced a multiple instance learning framework for feature representation in medical imaging, but their model is designed specifically for classification, and only applies to histopathology images. You et al. [50] presented CVRL, a semi-supervised approach for voxel-wise representations, which is designed for image segmentation, but requires CT inputs to extract anatomical information. SAM [48] is a self-supervised framework to encode anatomical information from CT images for feature embeddings, which has shown to be effective in downstream tasks such as registration (SAMConvex [29]). However, same as CVRL, SAM only works on CT. BrainPrint [42] is a compact and discriminative representation of brain morphology, which is specifically designed for cortical surface analyses. To our best knowledge, CIFL [11] is the only existing work on learning contrast-agnostic and task-independent brain feature representations. CIFL relies on contrastive learning alone, and is insufficient to outperform task/contrast-specific supervised models in downstream applications as shown by our experiments (Tab. 2).

**Contrast-agnostic Learning for MR Images** MRI scans acquired across sites vary substantially in contrasts, resolutions, orientations, etc. When given a new dataset,

<sup>1</sup><https://monai.io/model-zoo.html>

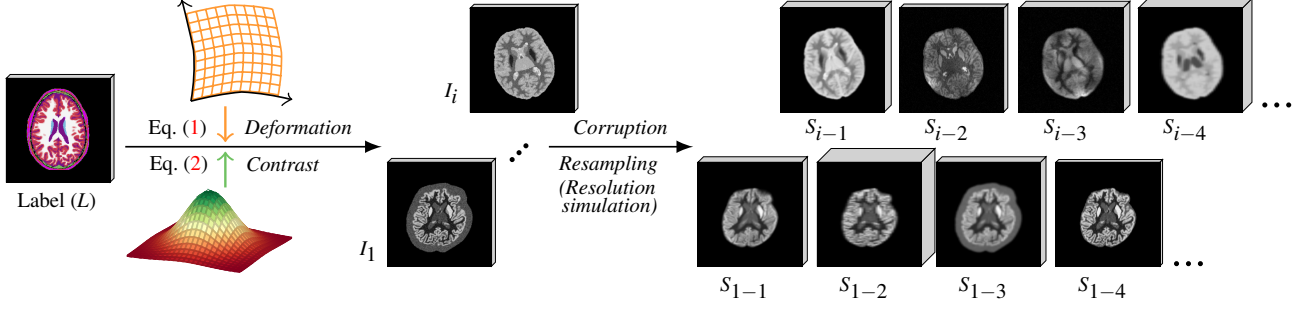


Figure 2. Brain-ID’s data simulation and augmentation process on the fly. Given the brain segmentation labels of a selected training identity/subject, we randomly generate its deformation field, and augment the sample with various contrast intensities and corruption levels.

heterogeneity leads to duplicate training efforts for approaches that are sensitive to specific combinations of MR contrast/resolution/orientation. Classical approaches in brain segmentation used Bayesian inference for contrast-robustness [16, 28], which requires a long processing time and struggles with resolutions that are not high and isotropic [21, 35]. Recently, SynthSeg [3] was proposed for contrast-agnostic segmentation and achieves impressive results with a synthetic generator that simulates widely diverse contrasts and avoids real data during training. Meanwhile, there have been works with similar ideas of using synthetic data to achieve contrast-invariance in tasks like image registration [19], super-resolution [22], and skull-stripping [20]. However, all the above-mentioned methods are trained in a task-specific manner, whose features therefore cannot be straightforwardly applied to other domains.

### 3. Method

As discussed in Sec. 1, the main challenges to obtain a general and robust feature representation for MR imaging lie in: (i) the practical restrictions of building large-scale datasets with diverse contrasts; and (ii) the nature of most medical imaging models that are highly task-oriented and trained on the specific choice of data (contrast, resolution, orientation, etc). In Brain-ID, our goal is to learn a general feature representation for brain imaging that is:

- (i) *Robust*: the resulting features should be robust to the anatomical structure of each identity (subject), and invariant to poses/deformations, contrasts, resolutions, and artifacts.
- (ii) *Expressive*: beyond being robust, the resulting features should also be sufficiently expressive and contain rich information, such that they could later be easily and effectively adapted to any potential downstream task.

In this section, we first introduce Brain-ID’s data generator (Sec. 3.1) and training strategy (Sec. 3.2) in order to achieve the above two aims. We then provide strategies for adapting Brain-ID’s resulting features to downstream tasks that could be either dependent or independent of the

contrast of input images (Sec. 3.3).

#### 3.1. Simulate to Enrich the Learning Space

A good representation relies on large-scale data, however, different acquisition protocols, processing pipelines, and privacy requirements across institutions make large-scale data less accessible and require significantly more effort. Moreover, for each identity/subject, there are usually only limited acquired images/modalities available. The lack of data consistency and intra-subject diversity are significant barriers to obtaining an identity-robust, contrast-invariant feature representation. Brain-ID avoids these barriers through the use of synthetic data.

In order to simulate images with complex brain structures, we follow SynthSR [22] and start from high-resolution brain segmentation images that provide labels of brain structures and extracerebral regions ( $L$  in Fig. 2). The simulation process consists of three separate steps, (i) deformation generation, (ii) contrast simulation, and (iii) data corruption (including models of lower resolution). For simplicity, we denote  $\Theta$  as the controlling parameter group of the simulation process described below.

**Deformation Simulation** We first generate a random deformation field ( $\phi|_{\theta_\phi}$ ) that is composed of an affine transformation followed by a non-linear displacement field:

$$\phi|_{\theta_\phi} = \mathcal{T}|_{\theta_\phi} \circ \mathcal{A}|_{\theta_\phi}, \quad (1)$$

where  $\mathcal{A}|_{\theta_\phi}$  denotes an affine transformation matrix which includes linear (rotation, scaling, shearing) transformation and translation,  $\mathcal{T}|_{\theta_\phi}$  refers to a non-linear displacement field computed as the integration of a stationary velocity field (SVF) that is smooth and invertible everywhere and thus preserves the topology of the brain anatomy [22].  $\theta_\phi \in \Theta$  controls the transformation ranges.

**MR Contrast Simulation** Then, we simulate high-resolution (HR) images ( $I(x), x \in \Omega$ ) by randomly “painting” intensities on the segmentation maps according to their

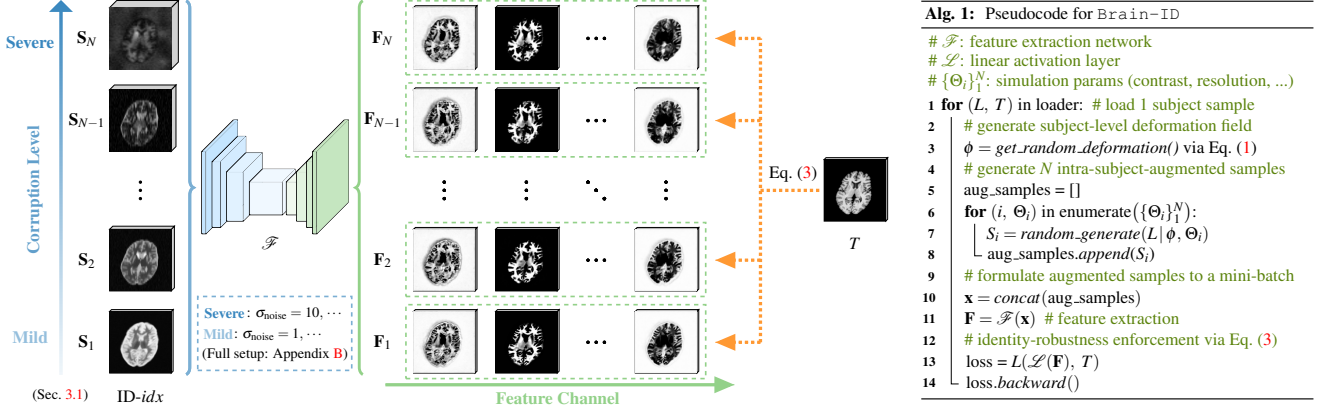


Figure 3. Overview of Brain-ID’s feature representation learning strategy (Sec. 3.2).

brain structure labels ( $l \in L$ ). Specifically, the regional intensities are generated by separately sampling a Gaussian distribution on each labeled region:

$$\begin{cases} I(x) \sim \mathcal{N}(\mu_l, \sigma_l), & l \in L, \\ \mu_l \sim \mathcal{N}(0, 1 | \theta_\mu, \theta_l), & \sigma_l \sim \mathcal{N}(0, 1 | \theta_\sigma, \theta_l), \end{cases} \quad (2)$$

where  $\mu_l$  and  $\sigma_l$  refer to the mean and standard deviation of each segmentation label  $l$ , and are independently sampled from Gaussian distributions at each voxel, with  $\theta_l, \theta_\mu, \theta_\sigma \in \Theta$  controlling the shifts and scales of their values.

**Resolution Simulation and Data Corruption** Given a deformed, contrast-simulated image ( $I$ ), we follow the data corruption pipeline in [21], which augments the image with different levels of resolution and scanning artifacts that are commonly found in clinical protocols, e.g., bias fields, slice spacing and thickness, partial voluming (PV), noise, etc.

As illustrated in Fig. 2, we are able to generate an infinite number of variations from a single identity with its unique structure labels. By generating images with randomized contrast/resolution/orientation on the fly for each identity, we enormously enrich the learning space for a robust representation, and focus the learning on intrinsic subject-specific features rather than superficial aspects of images that depend on acquisition parameters and conditions. In Sec. 4.5, we further conduct experiments to provide insights on how different choices of data augmentation/corruption levels would affect the robustness of Brain-ID features.

### 3.2. Extract Robust and Expressive Features

As mentioned above, we would like the resulting features from Brain-ID to be both robust to intra-identity variations and expressive to potential downstream tasks. In this section, we introduce Brain-ID’s training strategy to achieve the two desired feature representation properties.

**Intra-subject Sampling** In order to learn a feature representation that is consistent with each identity and robust to varying MR contrasts, we observe that augmenting *intra*-subject samples leads to better performance (Tab. 3). Specifically, instead of sampling multiple subjects for a mini-batch during each training iteration as in usual practice, Brain-ID focuses on maximizing the intra-subject variance to improve the identity-robustness of resulting features. As described in Alg. 1 (line 4-10), for each training iteration, after randomly sampling a subject and generating its deformation, Brain-ID creates a mini-batch of intra-subject augmentation samples ( $\{S_1, \dots, S_N\}$ ) with randomly generated contrasts, resolutions and corruptions (Sec. 3.1). As will be introduced in the following section, Brain-ID collects losses from all intra-subject augmented samples and conducts back-propagation *at once*, to encourage the identity-robustness of its learned features.

In Brain-ID, we set the samples generated within a mini-batch to have randomly painted contrasts and an *increasing* level of corruptions (Fig. 3 (left)), to maximize the intra-subject variance while ensuring the stability of the training process against extreme corruption levels. In Sec. 4.5, we compare various sampling strategies, and provide insights on preventing unstable training.

**Anatomy-guided Feature Representation** A richer learning space is helpful for improving the representation robustness against the variance of sample appearances, but not enough for extracting expressive features. For example, a mapping that projects all inputs to zero is perfectly robust, but it does not provide any useful information for potential downstream tasks. Therefore, proper guidance is crucial for feature representation as well. In CIFL [11], the authors use a contrastive loss on feature channels to encourage a more discriminative feature representation. However, this strategy is not sufficient, given the extremely complex nature of the human brain anatomy (see experimental comparisons



in Sec. 4). Instead, we propose to use the standard T1-weighted high-resolution structural MR contrast for brain morphometry, i.e., MP-RAGE (magnetization-prepared rapid gradient-echo), as the identity’s anatomy target to guide Brain-ID’s feature representation learning.

Specifically, as shown in Fig. 3, the feature extraction backbone ( $\mathcal{F}$ ) first maps the input mini-batch of intra-subject augmentation samples,  $\{S_1, \dots, S_N\}$ , to their corresponding feature space,  $\{\mathbf{F}_1, \dots, \mathbf{F}_N\}$ . An additional linear activation layer ( $\mathcal{L}$ ) then projects the features to the current identity/subject’s standard contrast (MP-RAGE) space,  $T$ . The overall training loss is obtained by summing over the standard contrast reconstruction loss of all intra-subject samples in the current mini-batch:

$$L = \sum_i^N |\mathcal{L}(\mathbf{F}_i) - T| + \lambda |\nabla \mathcal{L}(\mathbf{F}_i) - \nabla T|, \lambda \in R^+, \quad (3)$$

where  $T$ , as the high-resolution, unique anatomy target for all intra-subject samples, encourages the *similarities* of the features extracted from the same identity/subject via reconstruction (1<sup>st</sup> term) and gradient difference (2<sup>nd</sup> term)  $\ell_1$  loss. Brain-ID uses MP-RAGE as the supervision target, which formulates both super-resolution and contrast-synthesis problems, and encourages a richer feature representation. Sec. 4.5 provides further insights on how different choices of identity supervision guidance would affect the resulting features’ properties.

### 3.3. Adapting Brain-ID to Downstream Tasks

With the intra-subject augmentation and anatomy-guided feature learning design introduced in Sec. 3.2, a well-trained Brain-ID model is able to extract robust, high-resolution anatomical features from images with varying deformations, contrasts, resolutions, and artifacts. To minimize the modifications, here, we provide simple *one-layer* solutions to adapting Brain-ID features to various brain imaging applications. We later demonstrate that the following straightforward adaptations are effective enough for Brain-ID to achieve state-of-the-art performance across all downstream tasks, even for small datasets (Sec. 4.3-4.4).

**Contrast-independent Tasks** For tasks where the output should be independent of the input MR contrast, e.g., brain segmentation, we simply add an additional layer following Brain-ID features ( $\mathbf{F}$ ), and fine-tune the model:

$$L = \text{task\_loss\_func}(\mathcal{L}(\mathbf{F}), T), \quad (4)$$

where  $\mathcal{L}$  and  $T$  refer to the task-specific activation layer and the contrast-independent ground truth, respectively.

**Contrast-dependent Tasks** Since Brain-ID features are contrast-agnostic and robust to artifacts, for tasks relevant to the input’s contrast/quality, e.g., super-resolution,

we concatenate the input image ( $I$ ) that contains the original contrast information with its high-resolution Brain-ID features along the channel dimension, before forwarding into the task-specific activation layer:

$$L = \text{task\_loss\_func}(\mathcal{L}(\mathbf{F} \oplus I), T), \quad (5)$$

where  $\mathcal{L}$  and  $T$  refer to the task-specific activation layer and the contrast-dependent ground truth, respectively.

## 4. Experiments

In this section, we conduct experiments to demonstrate the two properties of Brain-ID as claimed in Sec. 3: (i) robustness (Sec. 4.2), which includes intra- and inter-subject feature evaluations; and (ii) expressiveness (Sec. 4.3), where we evaluate the performance of adapting Brain-ID features to a series of common brain imaging applications. We further challenge Brain-ID with reduced-size datasets to explore its ability to adapt when only a small amount of real data is available for fine-tuning (Sec. 4.4).

### 4.1. Datasets and Models for Comparison

**Datasets and Metrics** We experiment on 6 public datasets (ADNI [23], ADNI3 [46], HCP [15], ADHD200 [6], AIBL [17], OASIS3 [27]), covering both MR (T1-weighted, T2-weighted, FLAIR) and CT images.

We use various metrics to evaluate individual tasks across different aspects. For feature similarity measurements, we use L1 distance, and (MS-) SSIM ((multi-scale) structural similarity) [30, 44, 45]. For reconstruction and super-resolution, we use L1, PSNR (peak signal-to-noise ratio) and (MS-) SSIM. For segmentation, we use Dice scores. For bias field estimation, we use the normalized  $\ell_2$  distance (norm-L2) to avoid possible arbitrary scalings from nonuniformity correction [12]. Appendix A contains further details on metrics and dataset preprocessing.

**Implementation Details** As a general feature representation strategy, Brain-ID can use any backbone to extract brain features. In this work, we use a five-level 3D UNet [36] as Brain-ID’s backbone for feature extraction, with 64 feature channels in the last layer. During feature pre-training (Sec. 3.2), a linear regression layer is added for anatomy supervision (Eq. (3)). During downstream adaptations, a task-specific activation layer is added as described in Sec. 3.3. More implemental details are in Appendix B.

### 4.2. Feature Robustness

In this section, we examine the robustness of Brain-ID features, i.e., the 64 features from the last layer. To make the results comparable and reproducible, we use our data generator (Sec. 3.1) to augment (deform and corrupt) 1000 testing samples from 100 randomly selected identities in

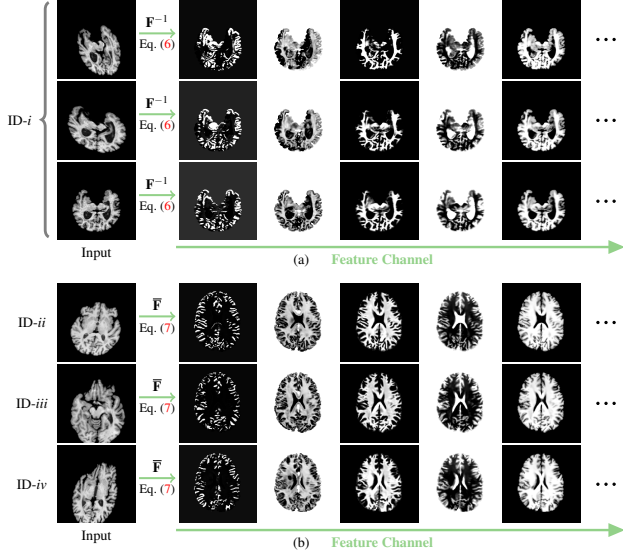


Figure 4. Qualitative results for (a) intra-subject and (b) inter-subject robustness evaluation of Brain-ID features.

Mode	Method	L1 ( $\downarrow$ )	SSIM ( $\uparrow$ )	MS-SSIM ( $\uparrow$ )
Intra	CIFL [11]	0.122 ( $\pm 0.031$ )	0.511 ( $\pm 0.298$ )	0.531 ( $\pm 0.367$ )
	Brain-ID	<b>0.011</b> ( $\pm 0.001$ )	<b>0.858</b> ( $\pm 0.041$ )	<b>0.921</b> ( $\pm 0.008$ )
Inter	CIFL [11]	0.230 ( $\pm 0.039$ )	0.552 ( $\pm 0.240$ )	0.524 ( $\pm 0.291$ )
	Brain-ID	<b>0.014</b> ( $\pm 0.013$ )	<b>0.843</b> ( $\pm 0.044$ )	<b>0.913</b> ( $\pm 0.011$ )

Table 1. Evaluations on intra/inter-subject feature robustness.

ADNI [23] (T1) testing set, with 10 intra-augmented samples for each identity. More setup details are in Appendix C.

We compare our features with CIFL [11] which is, to our best knowledge, the only similar work to Brain-ID, that also aims to learn contrast-agnostic brain features. Note the original CIFL method has only experimented on 2D images, and does not have our intra-subject sampling strategy for feature learning. Therefore, for a fairer comparison, we train CIFL feature representation following its proposed contrastive model design, while using the same synthetic data generator and training strategy as Brain-ID.

#### 4.2.1 Intra-subject Feature Robustness

Being robust to each identity/subject, ideally, Brain-ID features computed from the same subject should be structurally *identical*, regardless of the appearances of the inputs (contrast, resolution, noises, etc). To assess the similarity of predicted features from inputs ( $S$ ) of the same identity (ID) yet with different deformations and appearances, we first define their corresponding “canonical” features.

**“Canonical” Features** We compute  $\phi^{-1}$ , the inverse of  $S$  simulated deformation as in Eq. (1), and map back each sample’s ( $S$ ) Brain-ID features ( $F = F(S|\phi)$ ) to their

original domain without deformation augmentation:

$$F^{-1} = \phi^{-1} \circ F(S|\phi). \quad (6)$$

As shown in Fig. 4-(a), for the same identity ID- $i$ , although the input samples (row) have been augmented with different deformations and corruptions, their Brain-ID’s “canonical” features are of similar looking along each feature channel (column). In Tab. 1, we measure the feature similarity quantitatively. Specifically, for each testing identity, we first generate a sample *without* any deformation or corruption and use its Brain-ID feature as the gold-standard reference for all other “canonical” features computed from intra-subject augmented samples that may have different levels of deformation and corruptions. The final results are obtained by scores averaged over all 64 feature channels of all the intra-augmented samples.

#### 4.2.2 Inter-subject Feature Robustness

We also measure the feature robustness among different identities/anatomies, based on the assumption that features from different subjects should ideally be *structurally similar*, once being registered to a common domain.

**“Atlas-registered” Features** We register<sup>2</sup> features ( $F = F(S|\phi)$ ) from all identities to a common brain atlas<sup>3</sup>:

$$\bar{F} = \psi_{S \rightarrow A} \circ F(S|\phi), \quad (7)$$

where  $\psi_{S \rightarrow A}$  denotes the mapping from  $S$  to the atlas,  $A$ .

As shown in Fig. 4-(b), even though the input samples (row) from different identities have varying anatomical structures, after being registered to a common domain, their “atlas-registered” Brain-ID features still appear consistent (column). In Tab. 1, we further provide quantitative results of the structural similarity measured between features from different identities. Similar to Sec. 4.2.1, we randomly select a testing subject and generate a sample *without* any deformation or corruption. We use its “atlas-registered” Brain-ID feature as the gold standard for all “atlas-registered” features computed from other samples that may have different levels of deformation and corruption. The final results are obtained by scores averaged over all samples of the 100 testing identities.

In both intra/inter-subject aspects, Brain-ID outperforms CIFL by a large margin, which validates its feature robustness against deformations, contrasts, resolutions, artifacts (intra-subject), and anatomy (inter-subject). The robustness could potentially be useful for registration as well.

#### 4.3. Downstream Evaluation

Following the standard evaluation protocol for feature representation learning [8], we initialize networks with

<sup>2</sup>NiftyReg [32]: affine followed by non-rigid registration

<sup>3</sup>ICBM 2009a nonlinear symmetric MRI template

Modality (Contrast)	Dataset (Train/Test)	Method	Reconstruction				Segmentation Dice (↑)	Super-resolution (from 3 / 5 / 7 mm)			Bias Field norm-L2 (↓)
			L1 (↓)	PSNR (↑)	SSIM (↑)	MS-SSIM (↑)		PSNR (↑)	SSIM (↑)	MS-SSIM (↑)	
MR (T1)	ADNI [23] (1841/204)	FastSurfer [18]	-	-	-	-	0.803	-	-	-	-
		SAMSEG [9]	-	-	-	-	0.795	-	-	-	-
		SynthSR [21]	0.014	26.78	0.980	0.980	-	27.01 / 25.81 / 21.79	0.977 / 0.960 / 0.857	0.981 / 0.973 / 0.869	-
		CIFL [11]	0.013	26.97	0.973	0.961	0.820	30.12 / 27.21 / 23.80	0.978 / 0.912 / 0.887	0.979 / 0.950 / 0.842	0.053
		SCR	<b>0.011</b>	27.54	0.979	0.957	0.816	30.29 / 27.94 / 24.57	0.975 / 0.959 / 0.920	0.982 / 0.964 / 0.866	0.056
		Brain-ID	0.012	<b>33.82</b>	<b>0.993</b>	<b>0.989</b>	<b>0.837</b>	<b>31.30 / 28.62 / 24.68</b>	<b>0.983 / 0.961 / 0.928</b>	<b>0.987 / 0.980 / 0.947</b>	<b>0.048</b>
	HCP [15] (808/87)	FastSurfer [18]	-	-	-	-	0.819	-	-	-	-
		SAMSEG [9]	-	-	-	-	0.810	-	-	-	-
		SynthSR [21]	0.033	22.13	0.854	0.901	-	22.21 / 20.83 / 19.93	0.848 / 0.802 / 0.747	0.899 / 0.864 / 0.789	-
		CIFL [11]	0.029	26.42	0.932	0.913	0.804	25.98 / 25.11 / 23.99	0.930 / 0.883 / 0.871	0.936 / 0.927 / 0.880	0.059
		SCR	0.023	27.32	0.923	0.909	0.792	26.69 / 26.41 / 25.05	0.932 / 0.896 / 0.848	0.942 / 0.930 / <b>0.892</b>	0.069
		Brain-ID	<b>0.020</b>	<b>27.47</b>	<b>0.957</b>	<b>0.929</b>	<b>0.843</b>	<b>29.70 / 27.90 / 26.12</b>	<b>0.957 / 0.901 / 0.883</b>	<b>0.973 / 0.938 / 0.890</b>	<b>0.047</b>
	ADNI3 [46] (298/33)	FastSurfer [18]	-	-	-	-	0.796	-	-	-	-
		SAMSEG [9]	-	-	-	-	0.769	-	-	-	-
		SynthSR [21]	0.023	23.60	0.928	0.909	-	23.13 / 22.40 / 22.27	0.921 / 0.907 / 0.876	0.903 / 0.892 / 0.871	-
		CIFL [11]	0.028	28.52	0.961	0.970	0.819	27.81 / 27.10 / 26.32	0.900 / 0.877 / 0.864	0.812 / 0.793 / 0.769	0.102
		SCR	0.033	27.28	0.957	0.963	0.816	27.99 / 27.37 / 26.63	0.893 / 0.889 / 0.876	0.794 / 0.785 / 0.753	0.128
		Brain-ID	<b>0.021</b>	<b>29.89</b>	<b>0.966</b>	<b>0.976</b>	<b>0.843</b>	<b>30.17 / 28.23 / 26.89</b>	<b>0.962 / 0.923 / 0.892</b>	<b>0.973 / 0.901 / 0.883</b>	<b>0.093</b>
	ADHD200 [6] (865/96)	FastSurfer [18]	-	-	-	-	0.801	-	-	-	-
		SAMSEG [9]	-	-	-	-	0.784	-	-	-	-
		SynthSR [21]	0.035	21.67	0.882	0.853	-	21.42 / 21.13 / 21.41	0.876 / 0.857 / 0.809	0.851 / 0.845 / 0.805	-
		CIFL [11]	0.013	28.69	0.932	0.921	0.810	28.11 / 26.12 / 25.11	0.865 / 0.848 / <b>0.831</b>	0.828 / 0.800 / 0.789	0.109
		SCR	<b>0.011</b>	31.55	0.986	0.985	0.796	29.41 / 27.89 / 26.58	0.858 / 0.847 / 0.814	0.853 / 0.845 / <b>0.827</b>	0.113
		Brain-ID	<b>0.011</b>	<b>32.48</b>	<b>0.996</b>	<b>0.996</b>	<b>0.847</b>	<b>29.50 / 28.56 / 26.87</b>	<b>0.898 / 0.862 / 0.811</b>	<b>0.887 / 0.850 / 0.823</b>	<b>0.107</b>
	AIBL [17] (601/67)	FastSurfer [18]	-	-	-	-	0.802	-	-	-	-
		SAMSEG [9]	-	-	-	-	0.799	-	-	-	-
		SynthSR [21]	0.026	22.95	0.916	0.912	-	22.57 / 21.82 / 21.78	0.917 / 0.892 / 0.856	0.906 / 0.893 / 0.869	-
		CIFL [11]	0.011	30.12	0.938	0.925	0.816	29.46 / 27.97 / 26.73	0.907 / 0.889 / 0.870	0.891 / 0.872 / 0.857	0.094
		SCR	0.011	30.53	0.932	0.913	0.814	29.43 / 28.10 / 26.82	0.900 / 0.886 / 0.863	0.884 / 0.870 / 0.853	0.128
		Brain-ID	<b>0.009</b>	<b>33.73</b>	<b>0.972</b>	<b>0.963</b>	<b>0.851</b>	<b>29.75 / 28.58 / 27.09</b>	<b>0.957 / 0.922 / 0.890</b>	<b>0.975 / 0.956 / 0.937</b>	<b>0.088</b>
MR (T2)	HCP [15] (808/87)	SAMSEG [9]	-	-	-	-	0.782	-	-	-	-
		SynthSR [21]	0.034	21.46	0.833	0.885	-	-	-	-	-
		CIFL [11]	0.036	25.12	0.891	0.879	0.787	28.26 / 25.78 / 21.73	<b>0.959</b> / 0.893 / 0.797	0.982 / 0.906 / 0.742	0.138
		SCR	0.038	24.99	0.873	0.866	0.756	28.12 / 24.52 / 21.58	0.945 / 0.863 / 0.783	0.980 / 0.893 / 0.738	<b>0.136</b>
		Brain-ID	<b>0.016</b>	<b>28.10</b>	<b>0.934</b>	<b>0.935</b>	<b>0.805</b>	<b>30.26 / 26.11 / 24.10</b>	<b>0.959 / 0.902 / 0.832</b>	<b>0.987 / 0.953 / 0.912</b>	<b>0.136</b>
		SAMSEG [9]	-	-	-	-	0.763	-	-	-	-
	AIBL [17] (272/30)	SynthSR [21]	0.033	20.08	0.805	0.831	-	-	-	-	-
		CIFL [11]	0.022	23.71	0.820	0.839	0.721	29.98 / 27.01 / 25.66	0.931 / 0.899 / 0.861	0.967 / 0.941 / 0.905	0.193
		SCR	<b>0.020</b>	22.27	0.849	0.851	0.714	31.91 / 29.20 / <b>27.35</b>	0.954 / 0.934 / 0.896	0.982 / 0.969 / 0.947	0.197
		Brain-ID	0.022	<b>23.99</b>	<b>0.861</b>	<b>0.850</b>	<b>0.782</b>	<b>32.26 / 29.90 / 27.09</b>	<b>0.973 / 0.937 / 0.900</b>	<b>0.988 / 0.971 / 0.948</b>	<b>0.148</b>
MR (FLAIR)	ADNI3 [46] (298/33)	SAMSEG [9]	-	-	-	-	0.718	-	-	-	-
		SynthSR [21]	0.026	22.77	0.919	<b>0.900</b>	-	-	-	-	-
		CIFL [11]	0.020	21.29	0.911	0.897	0.761	<b>32.72</b> / 29.00 / 26.99	0.949 / 0.906 / 0.873	0.953 / 0.919 / 0.889	0.237
		SCR	0.025	20.80	0.901	0.862	0.759	32.36 / 28.71 / 28.00	0.945 / 0.915 / 0.877	0.941 / 0.936 / 0.917	0.236
		Brain-ID	<b>0.017</b>	<b>26.44</b>	<b>0.927</b>	0.892	<b>0.786</b>	<b>31.18 / 30.00 / 28.28</b>	<b>0.959 / 0.921 / 0.883</b>	<b>0.982 / 0.965 / 0.921</b>	<b>0.227</b>
		SAMSEG [9]	-	-	-	-	0.710	-	-	-	-
	AIBL [17] (302/34)	SynthSR [21]	0.029	21.77	0.902	0.892	-	-	-	-	-
		CIFL [11]	0.026	27.11	0.901	0.870	0.721	27.72 / 26.85 / 25.99	0.851 / 0.828 / 0.804	0.939 / 0.905 / 0.901	0.109
		SCR	0.023	26.84	0.898	0.867	0.720	28.02 / 26.52 / 25.43	0.878 / 0.838 / 0.799	0.943 / 0.901 / 0.891	0.115
		Brain-ID	<b>0.019</b>	<b>27.25</b>	<b>0.936</b>	<b>0.912</b>	<b>0.767</b>	<b>28.69 / 27.63 / 26.69</b>	<b>0.949 / 0.906 / 0.866</b>	<b>0.971 / 0.925 / 0.916</b>	<b>0.103</b>
CT	OASIS3 [27] (795/88)	SAMSEG [9]	-	-	-	-	0.701	-	-	-	-
		SynthSR [21]	0.041	20.93	0.758	0.786	-	-	-	-	-
		CIFL [11]	0.027	24.91	0.819	0.871	0.718	25.99 / 23.70 / 22.83	0.909 / <b>0.820</b> / 0.779	0.969 / 0.816 / 0.775	-
		SCR	0.025	24.35	0.811	0.872	0.709	26.34 / 23.64 / 22.62	0.905 / 0.818 / 0.770	0.873 / 0.818 / 0.780	-
		Brain-ID	<b>0.023</b>	<b>25.49</b>	<b>0.891</b>	<b>0.895</b>	<b>0.765</b>	<b>26.74 / 24.01 / 23.09</b>	<b>0.910 / 0.818 / 0.792</b>	<b>0.974 / 0.824 / 0.799</b>	-

(1) “-” means the model not applicable to current task/dataset: FastSurfer [18] and SAMSEG [9] are for segmentation-only; SynthSR [21] is designed for T1 weighted MRI synthesis; CT images do not have bias fields.  
(2) Note that SynthSR [21] is specifically designed to be biased towards higher values in white matter, therefore it normally results in lower PSNR scores.

Table 2. Quantitative comparisons of Brain-ID’s feature evaluation with state-of-the-art approaches on anatomy reconstruction, brain segmentation, super-resolution, and bias field estimation. (“train/test” corresponds to the number of subjects in the training/testing set.)

Brain-ID pre-trained weights and adapt them for each downstream task (Sec. 3.3). More details about training recipes and experimental results are in Appendix D.

**Models** To demonstrate the effectiveness of Brain-ID features, we compare Brain-ID’s downstream performance with: (i-ii) FastSurfer [18] (only works on T1-weighted MRI) and SAMSEG [9, 35], state-of-the-art brain segmentation approaches; (iii) SynthSR [21], a state-of-the-art, contrast-agnostic reconstruction and super-resolution model, which produces 1 mm T1-weighted MRI; (iv) SCR: a baseline model with the same architecture and augmentation strategy as Brain-ID, yet is trained from

*scratch* for each task and dataset. We use SCR to illustrate the effectiveness of Brain-ID features. (v) CIFL [11]: a baseline model with the same architecture/augmentation with Brain-ID and SCR, yet initialized with CIFL’s pre-trained features. We use CIFL to demonstrate the superiority of Brain-ID feature representation.

### 4.3.1 Contrast-independent Applications

**Anatomy Reconstruction/Contrast Synthesis** As one of the most common types of MRI scans, T1-weighted MR images highlight the differences between gray and white matter, and are mostly often utilized to image the anatomy

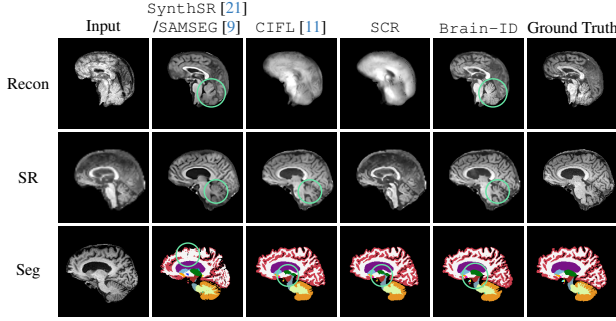


Figure 5. Qualitative comparisons on downstream tasks of reconstruction (Recon), super-resolution (SR), and segmentation (Seg), between Brain-ID, the baseline SCR, and the state-of-the-art methods CIFL [11], SynthSR [21] (Recon and SR), SAMSEG [9] (Seg). The testing examples are taken from small datasets: AIBL-FLAIR [17] for Recon, AIBL-T1 [17] for SR, and ADNI3-T1 [46] for Seg. The green circles highlight some less noticeable details.

of the brain, spinal cord, bones and joints [38]. For each dataset, we train the compared models to reconstruct their T1-weighted MRI counterparts with the  $\ell_1$  loss.

**Brain Segmentation** For each dataset, we use SynthSeg<sup>4</sup> to obtain the segmentation labels with 30 brain anatomical regions [16], as the gold standard segmentation target. We train our compared models to predict the brain segmentation labels, with the soft dice loss and cross-entropy loss [3].

As shown in Fig. 5, Brain-ID clearly outperforms CIFL and SCR in the reconstruction task. More importantly, as highlighted by the green circles, it reveals the anatomy details in reconstruction and produces visually more fine-grained results than the strong state-of-the-art method SynthSR [21]. Brain-ID also achieves better segmentation results, especially in the smaller and more challenging regions. Quantitative comparisons are in Tab. 2, where Brain-ID obtains the best scores across most metrics. Notably, Brain-ID achieves greater gains over baseline models, SCR and CIFL, especially on smaller datasets (e.g., ADNI3-T1/FLAIR, AIBL-FLAIR, where Brain-ID’s robust and contrast-agnostic features help models quickly adapt to specific task and dataset. Further insights on Brain-ID’s downstream performance regarding dataset sizes are provided in Sec. 4.4.

### 4.3.2 Contrast-dependent Applications

We also evaluate Brain-ID on two brain imaging tasks that are dependent on the input modality/quality.

**Image Super-resolution** Super-resolution seeks to obtain the high-resolution volume of the input contrast. We use the standard 1mm isotropic images from all datasets as the ground truth high-resolution target, and follow the strategy

<sup>4</sup><https://surfer.nmr.mgh.harvard.edu/fswiki/SynthSeg>

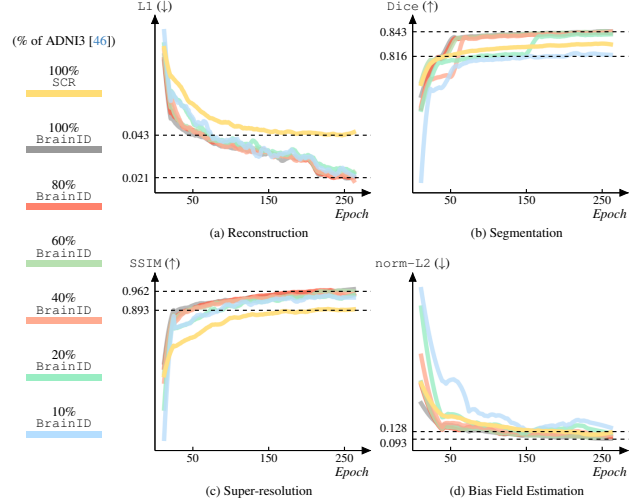


Figure 6. Adapting Brain-ID to small datasets. The horizontal (vertical) axes indicate training epochs (evaluation scores of corresponding tasks), “%” refers to the training set size compared to ADNI3 [46] full training set. Results are obtained by evaluating models collected throughout the epochs, on ADNI3 full testing set.

in SynthSR [21] where the input samples are randomly re-sampled and corrupted during training. During inference time, we downsample the original high-resolution images into 3mm, 5mm, and 7mm isotropic low-resolution images as inputs, and evaluate the quality of the output images.

**Bias Field Estimation** The bias field is a smooth, low-frequency multiplicative signal that corrupts MRI images, which affects image analysis tasks such as segmentation or texture analysis [24]. Bias field estimation is often needed as a pre-processing step to correct corrupted MRI images [12]. We augment the input samples with simulated bias fields (Sec. 3.1), and train the compared models with the  $\ell_2$  loss. During inference, we pre-generate and apply the bias fields on the testing data for reproducible results, and evaluate the bias field estimation performance.

With a simple contrast adaption (Sec. 3.3), the contrast-agnostic Brain-ID features still achieve state-of-the-art performance on contrast-dependent tasks (Tab. 2, Fig. 5), especially on relatively smaller datasets such as ADNI3-T1/FLAIR, AIBL-FLAIR. Brain-ID’s rich, high-resolution features greatly improve super-resolution, resulting in higher (MS-)SSIM scores. Brain-ID’s performance gains are less obvious in bias field estimation compared to other tasks, probably due to the fact that the bias field is approximately *independent* of brain anatomy.

## 4.4. Dealing with Small-size Datasets

To further explore the effectiveness of Brain-ID features when only limited real data is available for downstream applications, we evaluate Brain-ID and SCR on all the four



Model Setup [Comparison Target]	Feature Robustness (Intra)		Downstream (Reconstruction)		
	SSIM (↑)	MS-SSIM (↑)	L1 (↓)	PSNR (↑)	SSIM (↑)
[Representation guidance: supervision target for feature learning]					
Segmentation	<b>0.891</b>	<b>0.963</b>	0.029	28.13	0.958
Segmentation + MP-RAGE	0.863	0.940	0.023	29.05	0.964
MP-RAGE (Brain-ID)	0.858	0.921	<b>0.021</b>	<b>29.89</b>	<b>0.966</b>
[Sampling strategy: corruption levels in intra-subject mini-batches]					
All Mild ( $\sigma_{\text{noise}} = 1, \dots$ )	0.792	0.813	0.028	28.30	0.960
All Medium ( $\sigma_{\text{noise}} = 5, \dots$ )	0.831	0.899	0.022	29.67	0.964
All Severe ( $\sigma_{\text{noise}} = 10, \dots$ )	N/A	N/A	N/A	N/A	N/A
Mild to Severe (Brain-ID)	<b>0.858</b>	<b>0.921</b>	<b>0.021</b>	<b>29.89</b>	<b>0.966</b>
[Mini-batch size: number of intra-subject augmentation samples]					
2	0.826	0.897	0.025	28.83	0.959
3	0.841	0.902	0.022	29.30	0.962
4 (Brain-ID)	0.858	0.921	<b>0.021</b>	29.89	<b>0.966</b>
5	<b>0.860</b>	<b>0.929</b>	<b>0.021</b>	<b>29.93</b>	0.965

Table 3. Comparison results of Brain-ID variants.

downstream tasks in Sec. 4.3, with a series of progressively reduced training sets from ADNI3 [46]. Specifically, we fine-tune Brain-ID on subsets of the ADNI3 training set, which has 298 training cases in total. As shown in Fig. 6, we reduce the training set size percentage from 100% of ADNI3 to an extreme 10%, respectively. With only 20% of the data (mint line), Brain-ID still achieves better performance compared to its full-sized baseline, “100%” SCR (yellow line), over all tasks. A training set of 30 samples (10%, blue line) may be at the edge of obtaining acceptable results for Brain-ID, as the model becomes less stable and the performance drops occur more frequently – especially for brain segmentation (Fig. 6-(b)).

#### 4.5. Additional Experimental Results

We conduct further comparisons on Brain-ID’s feature representation performance, in terms of different anatomical supervision choices, and varying training sampling strategies. More results and discussions are in Appendix E. **Identity Supervision Choice** As introduced in Sec. 3.2, Brain-ID proposes to use a high-resolution MP-RAGE scan as our anatomy guidance for brain feature representation. Here, we explore other potential targets that provide anatomical information: (i) segmentation labels; (ii) both segmentation labels and MP-RAGE. As shown in Tab. 3, adding segmentation task into the feature learning helps increase the feature robustness, yet inhibits the feature expressiveness and therefore affects the downstream performance; we observe features obtained from segmentation guidance produce less high-frequency texture than their Brain-ID counterparts, which carry richer information. (Please refer to the visualizations in Appendix E.)

**Training Sampling Strategy** Since Brain-ID features are entirely trained on synthetic data, it is crucial to set a proper augmentation range, i.e., enough to improve the feature robustness, but not too severe that harms the model’s stability. As shown in Tab. 3, training on batches with all mildly-corrupted intra-subject samples results in reduced feature robustness, and further affects the downstream performance. Meanwhile, using all extremely corrupted sam-

ples easily leads to an unstable training process and model collapse. We train Brain-ID with intra-subject samples of increasing corruptions (Fig. 3 (left)). Please refer to Appendix B for full parameter setups of all corruption levels.

**Batch Size** As described in Sec. 3.2, Brain-ID computes its training loss of all intra-subject samples in a mini-batch at once (Eq. (3)). We observe that larger batches help improve the feature robustness (Tab. 3), yet do not necessarily further enhance the downstream performance.

## 5. Conclusion

We present Brain-ID, a feature representation learning strategy for brain imaging that is robust to anatomy, and agnostic to contrast, orientation, resolution, artifacts, etc. Brain-ID is trained on synthetic data, and adapts to downstream tasks with an one-layer modification. We validate Brain-ID features’ robustness, and effectiveness on four applications (reconstruction, segmentation, super-resolution, bias field estimation). Experiments on 6 public datasets, including both MR and CT, demonstrate that Brain-ID achieves state-of-the-art performance in all tasks/modalities, and preserves high performance on small-size datasets. Future work will focus on robust registration from features, and pathology representation. We believe Brain-ID opens up the great potential of robust foundation models for non-calibrated image modalities like MR.

## Acknowledgments

This work was primarily supported by National Institutes of Health (NIH) under award number 1RF1AG080371. Additional funding was provided by NIH grants 1UM1MH130981, 1R01AG070988, 1RF1MH123195, 1R01EB031114 and by a grant from the Jack Satter Foundation.

## References

- [1] Muhammad Awais, Muzammal Naseer, Salman Siddique Khan, Rao Muhammad Anwer, Hisham Cholakkal, Mubarak Shah, et al. Foundational models defining a new era in vision: A survey and outlook. *arXiv*, abs/2307.13721, 2023. 2
- [2] Guha Balakrishnan, Amy Zhao, Mert Rory Sabuncu, John V. Guttag, and Adrian V. Dalca. Voxelmorph: A learning framework for deformable medical image registration. *IEEE Transactions on Medical Imaging*, 2018. 2
- [3] Benjamin Billot, Douglas N. Greve, Oula Puonti, Axel Thielscher, Koen Van Leemput, Bruce R. Fischl, et al. Synthseg: Segmentation of brain mri scans of any contrast and resolution without retraining. *Medical Image Analysis*, 2021. 2, 3, 8, 12
- [4] Rishi Bommasani, Drew A. Hudson, Ehsan Adeli, Russ Altman, Simran Arora, Sydney von Arx, et al. On the opportuni-

- ties and risks of foundation models. *arXiv*, abs/2108.07258, 2021. [2](#)
- [5] Michael N. Brant-Zawadzki, Gary D. Gillan, and Wolfgang R. Nitz. Mp rage: a three-dimensional, t1-weighted, gradient-echo sequence—initial experience in the brain. *Radiology*, 1992. [2](#)
- [6] Matthew R. G. Brown, Gagan Preet Singh Sidhu, Russell Greiner, Nasimeh Asgarian, Meysam Bastani, Peter H. Silverstone, et al. Adhd-200 global competition: diagnosing adhd using personal characteristic data can outperform resting state fmri measurements. *Frontiers in Systems Neuroscience*, 2012. [5](#), [7](#), [11](#)
- [7] Tom Brown, Benjamin Mann, Nick Ryder, Melanie Subbiah, Jared D Kaplan, Prafulla Dhariwal, Arvind Neelakantan, Pranav Shyam, Girish Sastry, Amanda Askell, et al. Language models are few-shot learners. In *NeurIPS*, 2020. [2](#)
- [8] Mathilde Caron, Hugo Touvron, Ishan Misra, Hervé Jégou, Julien Mairal, Piotr Bojanowski, and Armand Joulin. Emerging properties in self-supervised vision transformers. In *ICCV*, 2021. [6](#)
- [9] Stefano Cerri, Oula Puonti, Dominik S. Meier, Jens Wuerfel, Mark Mühlau, Hartwig Roman Siebner, and Koenraad Van Leemput. A contrast-adaptive method for simultaneous whole-brain and lesion segmentation in multiple sclerosis. *NeuroImage*, 2020. [7](#), [8](#), [13](#), [16](#)
- [10] Aakanksha Chowdhery, Sharan Narang, Jacob Devlin, Maarten Bosma, Gaurav Mishra, Adam Roberts, et al. Palm: Scaling language modeling with pathways. *JMLR*, 2022. [2](#)
- [11] Yue Zhi Russ Chua and Adrian V. Dalca. Contrast invariant feature representations for segmentation and registration of medical images. In *Medical Imaging with Deep Learning, short paper track*, 2023. [2](#), [4](#), [6](#), [7](#), [8](#), [15](#), [16](#)
- [12] Zin Yan Chua, Weili Zheng, Michael W. L. Chee, and Vitali Zagorodnov. Evaluation of performance metrics for bias field correction in mr brain images. *Journal of Magnetic Resonance Imaging*, 2009. [5](#), [8](#), [12](#)
- [13] Bob D. de Vos, Floris F. Berendsen, Max A. Viergever, Hesselam Sokooti, Marius Staring, and Ivana Išgum. A deep learning framework for unsupervised affine and deformable image registration. *Medical Image Analysis*, 2019. [2](#)
- [14] Zhipeng Ding, Xu Han, Peirong Liu, and Marc Niethammer. Local temperature scaling for probability calibration. In *ICCV*, 2021. [2](#)
- [15] David C. Van Essen, Kâmil Uğurbil, Edward J. Auerbach, Deanna M. Barch, Timothy Edward John Behrens, Richard D. Bucholz, et al. The human connectome project: A data acquisition perspective. *NeuroImage*, 2012. [5](#), [7](#), [11](#)
- [16] Bruce R. Fischl, David H. Salat, Evelina Busa, Marilyn S. Albert, Megan Dieterich, Christian Haselgrove, et al. Whole brain segmentation automated labeling of neuroanatomical structures in the human brain. *Neuron*, 2002. [3](#), [8](#)
- [17] Christopher Fowler, Stephanie R. Rainey-Smith, Sabine M. Bird, Julia Bomke, Pierrick T. Bourgeat, et al. Fifteen years of the australian imaging, biomarkers and lifestyle (aibl) study: Progress and observations from 2,359 older adults spanning the spectrum from cognitive normality to alzheimer’s disease. *Journal of Alzheimer’s Disease Reports*, 2021. [5](#), [7](#), [8](#), [11](#)
- [18] Leonie Henschel, Sailesh Conjeti, Santiago Estrada, Kersten Diers, Bruce R. Fischl, and Martin Reuter. FastSurfer - a fast and accurate deep learning based neuroimaging pipeline. *NeuroImage*, 2019. [7](#), [13](#)
- [19] Malte Hoffmann, Benjamin Billot, Douglas N. Greve, Juan Eugenio Iglesias, Bruce R. Fischl, and Adrian V. Dalca. Synthmorph: Learning contrast-invariant registration without acquired images. *IEEE Transactions on Medical Imaging*, 2020. [2](#), [3](#)
- [20] Andrew Hoopes, Jocelyn S. Mora, Adrian V. Dalca, Bruce R. Fischl, and Malte Hoffmann. Synthstrip: skull-stripping for any brain image. *NeuroImage*, 2022. [3](#), [12](#)
- [21] Juan Eugenio Iglesias, Benjamin Billot, Yael Balbastre, Colin G. Magdamo, Steve Arnold, Sudeshna Das, et al. Synths: A public ai tool to turn heterogeneous clinical brain scans into high-resolution t1-weighted images for 3d morphometry. *Science Advances*, 2023. [2](#), [3](#), [4](#), [7](#), [8](#), [13](#), [15](#)
- [22] Juan Eugenio Iglesias, Benjamin Billot, Yael Balbastre, Azadeh Tabari, John Conklin, Daniel C. Alexander, et al. Joint super-resolution and synthesis of 1 mm isotropic mp-rage volumes from clinical mri exams with scans of different orientation, resolution and contrast. *NeuroImage*, 2020. [2](#), [3](#)
- [23] Clifford R. Jack, Matt A. Bernstein, Nick C Fox, Paul M. Thompson, Gene E. Alexander, Danielle J. Harvey, et al. The alzheimer’s disease neuroimaging initiative (adni): Mri methods. *Journal of Magnetic Resonance Imaging*, 2008. [5](#), [6](#), [7](#), [11](#), [12](#), [13](#)
- [24] Jaber Juntu, Jan Sijbers, Dirk Van Dyck, and Jan Gielen. Bias field correction for mri images. In *International Conference on Computer Recognition Systems*, 2005. [8](#)
- [25] Konstantinos Kamnitsas, Christian Ledig, Virginia F. J. Newcombe, Joanna P. Simpson, Andrew D. Kane, David K. Menon, et al. Efficient multi-scale 3d cnn with fully connected crf for accurate brain lesion segmentation. *Medical Image Analysis*, 2016. [2](#)
- [26] Alexander Kirillov, Eric Mintun, Nikhila Ravi, Hanzi Mao, Chloe Rolland, Laura Gustafson, et al. Segment anything. *arXiv*, abs/2304.02643, 2023. [2](#)
- [27] Pamela J. LaMontagne, Sarah J. Keefe, Wallace Lauren, Chengjie Xiong, Elizabeth A. Grant, Krista L. Moulder, et al. Oasis-3: Longitudinal neuroimaging, clinical, and cognitive dataset for normal aging and alzheimer’s disease. *Alzheimer’s & Dementia*, 2018. [5](#), [7](#), [12](#)
- [28] Koenraad Van Leemput, Frederik Maes, Dirk Vandermeulen, and Paul Suetens. A unifying framework for partial volume segmentation of brain mr images. *IEEE Transactions on Medical Imaging*, 2003. [3](#)
- [29] Zi Li, Lin Tian, Tony C. W. Mok, Xiaoyu Bai, Puyang Wang, Jia Ge, et al. Samconvex: Fast discrete optimization for ct registration using self-supervised anatomical embedding and correlation pyramid. In *MICCAI*, 2023. [2](#)
- [30] Peirong Liu, Rui Wang, Xuefei Cao, Yipin Zhou, Ashish Shah, Maxime Oquab, Camille Couprie, and Ser Nam Lim. Self-appearance-aided differential evolution for motion transfer. *arXiv*, abs/2110.04658, 2021. [5](#), [12](#)
- [31] Fausto Milletari, Nassir Navab, and Seyed-Ahmad Ahmadi. V-net: Fully convolutional neural networks for volumetric medical image segmentation. *3DV*, 2016. [2](#)

- [32] Marc Modat, Gerard R. Ridgway, Zeike A. Taylor, Manja Lehmann, Josephine Barnes, David John Hawkes, et al. Fast free-form deformation using graphics processing units. *Computer Methods and Programs in Biomedicine*, 2010. 6, 12
- [33] Michael Moor, Oishi Banerjee, Zahra F H Abad, Harlan M. Krumholz, Jure Leskovec, Eric J. Topol, and Pranav Rajpurkar. Foundation models for generalist medical artificial intelligence. *Nature*, 2023. 2
- [34] Ralph-Axel Müller, Patricia Shih, Brandon Keehn, Janae Ruth Deyoe, K. M. Leyden, and Dinesh Shukla. Underconnected, but how? a survey of functional connectivity mri studies in autism spectrum disorders. *Cerebral Cortex*, 2011. 2
- [35] Oula Puonti, Juan Eugenio Iglesias, and Koenraad Van Leemput. Fast and sequence-adaptive whole-brain segmentation using parametric bayesian modeling. *NeuroImage*, 2016. 3, 7, 13
- [36] Olaf Ronneberger, Philipp Fischer, and Thomas Brox. U-net: Convolutional networks for biomedical image segmentation. In *MICCAI*, 2015. 2, 5, 12
- [37] Karan Singhal, Shekoofeh Azizi, Tao Tu, Said Mahdavi, Jason Wei, Hyung Won Chung, et al. Large language models encode clinical knowledge. *Nature*, 2022. 2
- [38] Mark R. Symms, Hans Rolf Jäger, Klaus Schmierer, and Tarek A. Yousry. A review of structural magnetic resonance neuroimaging. *Journal of Neurology, Neurosurgery & Psychiatry*, 2004. 8
- [39] Ryutaro Tanno, Daniel E. Worrall, Enrico Kaden, and Daniel C. Alexander. Uncertainty modelling in deep learning for safer neuroimage enhancement: Demonstration in diffusion mri. *NeuroImage*, 2020. 2
- [40] Qiyuan Tian, Berkin Bilgiç, Qiyyun Fan, Chanon Ngamsombat, Natalia Zaretskaya, Nina E. Fultz, et al. Improving in vivo human cerebral cortical surface reconstruction using data-driven super-resolution. *Cerebral Cortex*, 2020. 2
- [41] Tao Tu, Shekoofeh Azizi, Danny Driess, Mike Schaeckermann, Mohamed Amin, Pi-Chuan Chang, et al. Towards generalist biomedical ai. *arXiv*, abs/2307.14334, 2023. 2
- [42] Christian Wachinger, Polina Golland, and Martin Reuter. Brainprint : Identifying subjects by their brain. In *MICCAI*, 2014. 2
- [43] Mei Wang and Weihong Deng. Deep visual domain adaptation: A survey. *Neurocomputing*, 2018. 2
- [44] Ting-Chun Wang, Arun Mallya, and Ming-Yu Liu. One-shot free-view neural talking-head synthesis for video conferencing. In *CVPR*, 2021. 5, 12
- [45] Zhou Wang, Eero P Simoncelli, and Alan C Bovik. Multiscale structural similarity for image quality assessment. In *The Thirty-Seventh Asilomar Conference on Signals, Systems & Computers*, 2003, 2003. 5, 12
- [46] Michael W. Weiner, Dallas P Veitch, Paul S. Aisen, Laurel A Beckett, Nigel J. Cairns, Robert C. Green, et al. The alzheimer’s disease neuroimaging initiative 3: Continued innovation for clinical trial improvement. *Alzheimer’s & Dementia*, 2017. 5, 7, 8, 9, 11
- [47] Yan Xu, Tao Mo, Qiwei Feng, Peilin Zhong, Maode Lai, and Eric I-Chao Chang. Deep learning of feature representation with multiple instance learning for medical image analysis. In *ICASSP*, 2014. 2
- [48] Ke Yan, Jinzheng Cai, Dakai Jin, Shun Miao, Adam P. Harrison, Dazhou Guo, et al. Sam: Self-supervised learning of pixel-wise anatomical embeddings in radiological images. *IEEE Transactions on Medical Imaging*, 2020. 2
- [49] Xiao Yang, Roland Kwitt, and Marc Niethammer. Quicksilver: Fast predictive image registration – a deep learning approach. *NeuroImage*, 2017. 2
- [50] Chenyu You, Ruihan Zhao, Lawrence H. Staib, and James S. Duncan. Momentum contrastive voxel-wise representation learning for semi-supervised volumetric medical image segmentation. In *MICCAI*, 2021. 2
- [51] Yukun Zhou, Mark A Chia, Siegfried Karl Wagner, Murat S. Ayhan, Dominic J Williamson, Robbert R. Struyven, et al. A foundation model for generalizable disease detection from retinal images. *Nature*, 2023. 2

## Appendix

### A. Datasets and Metrics

**Datasets** We test and compare our method over various datasets including modalities of MR and CT, the MR images further contain T1-weighted, T2-weighted and FLAIR (fluid-attenuated inversion recovery) images.

- ADNI [23]: we use T1-weighted (2045 cases) MRI scans from the Alzheimer’s Disease Neuroimaging Initiative (ADNI). All scans are acquired at 1 mm isotropic resolution from a wide array of scanners and protocols. The dataset contains aging subjects, some diagnosed with mild cognitive impairment (MCI) or Alzheimer’s Disease (AD). Many subjects present strong atrophy patterns and white matter lesions.
- HCP [15]: we use T1-weighted (897 cases) and T2-weighted (897 cases) MRI scans of young subjects from the Human Connectome Project, acquired at 0.7 mm resolution.
- ADNI3 [46]: we use T1-weighted (331 cases) and FLAIR (331 cases) MRI scans from ADNI3, which continues the previously funded ADNI1, ADNI-GO, and ADNI2 studies to determine the relationships between the clinical, cognitive, imaging, genetic and biochemical biomarker characteristics of the entire spectrum of sporadic late onset AD.
- ADHD200 [6]: we use T1-weighted (961 cases) MRI scans from ADHD200 Sample, which is a grassroots initiative dedicated to the understanding of the neural basis of Attention Deficit Hyperactivity Disorder (ADHD).
- AIBL [17]: we use T1-weighted (668 cases), T2-weighted (302 cases) and FLAIR (336 cases) MRI scans from The Australian Imaging, Biomarkers and Lifestyle

(AIBL) Study, which is a study of cognitive impairment (MCI) and Alzheimer’s disease dementia.

- OASIS3 [27]: we use CT (885 cases) scans from OASIS3, which is a longitudinal neuroimaging, clinical, and cognitive dataset for normal aging and AD. For our experiments, we use CT and T1-weighted MRI pair with the earliest date, from each subject.

**Data for Synthetic Generator** Brain-ID’s synthetic generator uses (1) brain segmentation labels, for random-contrast input images generation (Sec. 3.1), and (2) MP-RAGE, the target ground truth for anatomy-guided supervision (Sec. 3.2). In this work, we use the segmentation maps of training images from ADNI [23], as well as their corresponding MP-RAGE images. Note that we do not use any type of real images from ADNI as input for Brain-ID’s pre-training.

**Data Preprocessing** For all datasets, we skull-strip all the images using SynthStrip [20], and resample them to 1 mm isotropic resolution. For all the images, except T1-weighted MRI, in each dataset, we use NiftyReg [32] rigid registration to register all images to their same-subject T1-weighted MRI counterparts. The gold-standard brain segmentation maps are obtained by performing SynthSeg [3] on the T1-weighted MR images of all the subjects.

**Metrics** We resort to various metrics for evaluating individual tasks across multiple aspects:

- L1: the average  $L1$  distance, is used for intra/inter-subject feature distance evaluation (Sec. 4.2), and the overall prediction correctness of anatomy reconstruction (Sec. 4.3.1), super-resolution and bias-field estimation (Sec. 4.3.2).
- normL2: the normalized  $L2$  distance for bias field [12] is defined as:

$$\text{normL2} = \sqrt{\frac{\sum_x (wB_{\text{est}}(x) - B_{\text{true}}(x))^2}{\sum_x B_{\text{true}}^2(x)}}, \quad (\text{A.1})$$

where  $w$  is the normalization coefficient obtained by:

$$w = \frac{\sum_x B_{\text{true}}(x)B_{\text{est}}(x)}{\sum_x B_{\text{est}}^2(x)}, \quad x \in \Omega, \quad (\text{A.2})$$

$\Omega$  refers to the brain domain,  $B_{\text{est}}$  and  $B_{\text{true}}$  are the estimated and ground truth bias fields, respectively. Normalization is necessary for the evaluation of bias field estimation (Sec. 4.3.2) because nonuniformity correction may result in arbitrary scaling of the bias field.

- PSNR: the peak signal-to-noise ratio (PSNR) that indicates the fidelity of predictions. It is used in anatomy reconstruction (Sec. 4.3.1) and super-resolution (Sec. 4.3.2).

- (MS-) SSIM: the structural similarity scores between the generated and real images. MS-SSIM is a variant of SSIM focusing on multiple scales of the images that are shown to correlate well with human perception [30, 44, 45]. They are used in intra/inter-subject feature distance evaluation (Sec. 4.2), reconstruction (Sec. 4.3.1), and super-resolution (Sec. 4.3.2),
- Dice: the similarity score between predicted and ground truth segmentations, and it is used in brain segmentation evaluation (Sec. 4.3.1).

## B. Implementation Details

**Model Architecture** As mentioned in Sec. 4, Brain-ID can use any backbone to extract brain features. We use the five-level 3D UNet [36] as Brain-ID’s backbone for feature extraction, with 64 feature channels in the last layer.

- During the feature pre-training stage (Sec. 3.2), a linear regression layer is added following the feature outputs for anatomy supervision (Eq. (3)).
- During downstream tasks adaptations, the regression layer for anatomy supervision is abandoned, instead, a task-specific activation layer is added following the feature outputs (Sec. 3.3). Specifically, a linear regression layer is added for the tasks, anatomy reconstruction/contrast synthesis, image super-resolution, and bias field estimation. An additional softmax activation is added for segmentation probability outputs.

**Feature Backbone Pre-training** We pre-train Brain-ID on the synthetic data from our generator (Sec. 3.1) for 300,000 iterations, with a patch size of  $128^3$  and a mini-batch size (i.e., number of intra-subject augmented samples) of 4. We use the synchronized AdamW optimization, with a base learning rate of  $10^{-4}$  and a linear warm-up in the first 2,000 iterations followed by a multi-step learning schedule (learning rate drops at 160,000 and 240,000 iterations) with a multiplier of 0.1.

**Synthetic Data Generator** As shown in Fig. 3, Brain-ID simulates its training samples of increasing corruption levels, from mild to severe. Tab. 3 also explores the effects of different levels of sample corruption on feature robustness and downstream performance. In Tab. B.1, we list the generator parameters for mild, medium, and severe data corruption levels, respectively. Note that (1) for each level, the setup parameters only control the corruption value ranges, since the simulation is randomized, there could still be mildly corrupted samples generated under the “severe” settings; (2) The random deformation fields are independent of data corruption levels.



Category	Param	Corruption Level		
		Mild	Medium	Severe
Deformation	$\text{affine-rotation}_{\max}$	15	=	=
	$\text{affine-shearing}_{\max}$	0.2	=	=
	$\text{affine-scaling}_{\max}$	0.2	=	=
	$\text{nonlinear-scale } \mu_{\min}$	0.03	=	=
	$\text{nonlinear-scale } \mu_{\max}$	0.06	=	=
	$\text{nonlinear-scale } \sigma_{\max}$	4	=	=
Resolution	$p_{\text{low-field}}$	0.1	0.3	0.5
	$p_{\text{anisotropic}}$	0	0.1	0.25
Bias Field	$\mu_{\min}$	0.01	0.02	0.02
	$\mu_{\max}$	0.02	0.03	0.04
	$\sigma_{\min}$	0.01	0.05	0.1
	$\sigma_{\max}$	0.05	0.3	0.6
	$\sigma_{\min}$	0.01	0.5	5
Noises	$\sigma_{\max}$	1	5	15

Table B.1. Brain-ID synthetic generator setups: mild, medium and severe levels.  $p$  denotes probability,  $\mu$  and  $\sigma$  refer to the mean and variance of the Gaussian distributions, respectively.

### C. Feature Robustness Evaluation

For the evaluation of feature robustness, we use T1-weighted MRI of 100 randomly selected identities from ADNI [23]. To challenge the model’s robustness against data corruptions, and meanwhile obtain comparable and reproducible results, we use our data generator (Sec. 3.1) to pre-augment all the input images. Note that in this section, there is no contrast simulation step within data augmentation, and only the random deformation and data corruptions are applied. For each selected identity/subject, we generate intra-augmented samples. All samples are generated with “medium” corruption settings as listed in Tab. B.1.

### D. Downstream Task Comparisons

For all the downstream tasks, the model architecture and training sampling strategy used for Brain-ID, SCR and CIFL are the same. The only difference between the three compared models lies in their initial weights. Brain-ID and CIFL are initialized by their pre-trained weights from training on synthetic data as described in Secs. 3.1 and 3.2.

For the state-of-the-art comparisons, we consider FastSurfer [18] and SAMSEG [9, 35] for brain segmentation, and SynthSR [21] for anatomy reconstruction/contrast synthesis and super-resolution for T1-weighted images.

- FastSurfer [18] is a state-of-the-art brain segmentation model, which is designed for segmentation on T1-weighted images. Therefore, we only report the segmentation performance of FastSurfer on T1-weighted MRI. In addition, since FastSurfer does not predict cerebrospinal fluid (CSF), we remove the CSF label during the Dice score computation.

- SAMSEG [9, 35] is a state-of-the-art, multi-modal brain segmentation model, which works on both MR and CT images. Similar to FastSurfer, SAMSEG does not predict the CSF label either, the CSF label is therefore removed during the Dice score computation of SAMSEG.
- SynthSR [21] is a state-of-the-art, contrast-agnostic model for anatomy reconstruction/contrast synthesis. For input MRI images with any contrast and resolution, SynthSR generates their corresponding high-resolution, 1 mm isotropic T1-weighted MRI. In our comparisons, we apply SynthSR on our anatomy reconstruction/contrast synthesis task, as well as the image super-resolution task of T1-weighted MRI.

### E. Additional Experimental Results

**Feature Representation Learning** As discussed in Sec. 4.5, in Brain-ID we adopt the high-resolution MP-RAGE scan as the anatomy guidance for brain feature representation. Experimental comparisons in Tab. 3 illustrate that incorporating segmentation as the target for anatomical supervision in learning brain feature representation leads to reduced high-frequency texture compared to the use of MP-RAGE alone. The visual comparisons presented in Fig. C.1 reveal that the features with segmentation guidance indeed encompass anatomical structures, however, they exhibit notably smoother texture *within* each structural region defined by the brain segmentation labels. In contrast, employing MP-RAGE as the target for anatomical supervision inherently entails the tasks of anatomy reconstruction and super-resolution simultaneously. The resulting features from Brain-ID are shown to carry richer information content, as evidenced by the more pronounced high-frequency textures they manifest.

**Downstream Task Evaluation** In addition to the qualitative results in Figs. 1 and 5, we provide more visualization comparisons of the downstream tasks in Figs. E.2 to E.4.

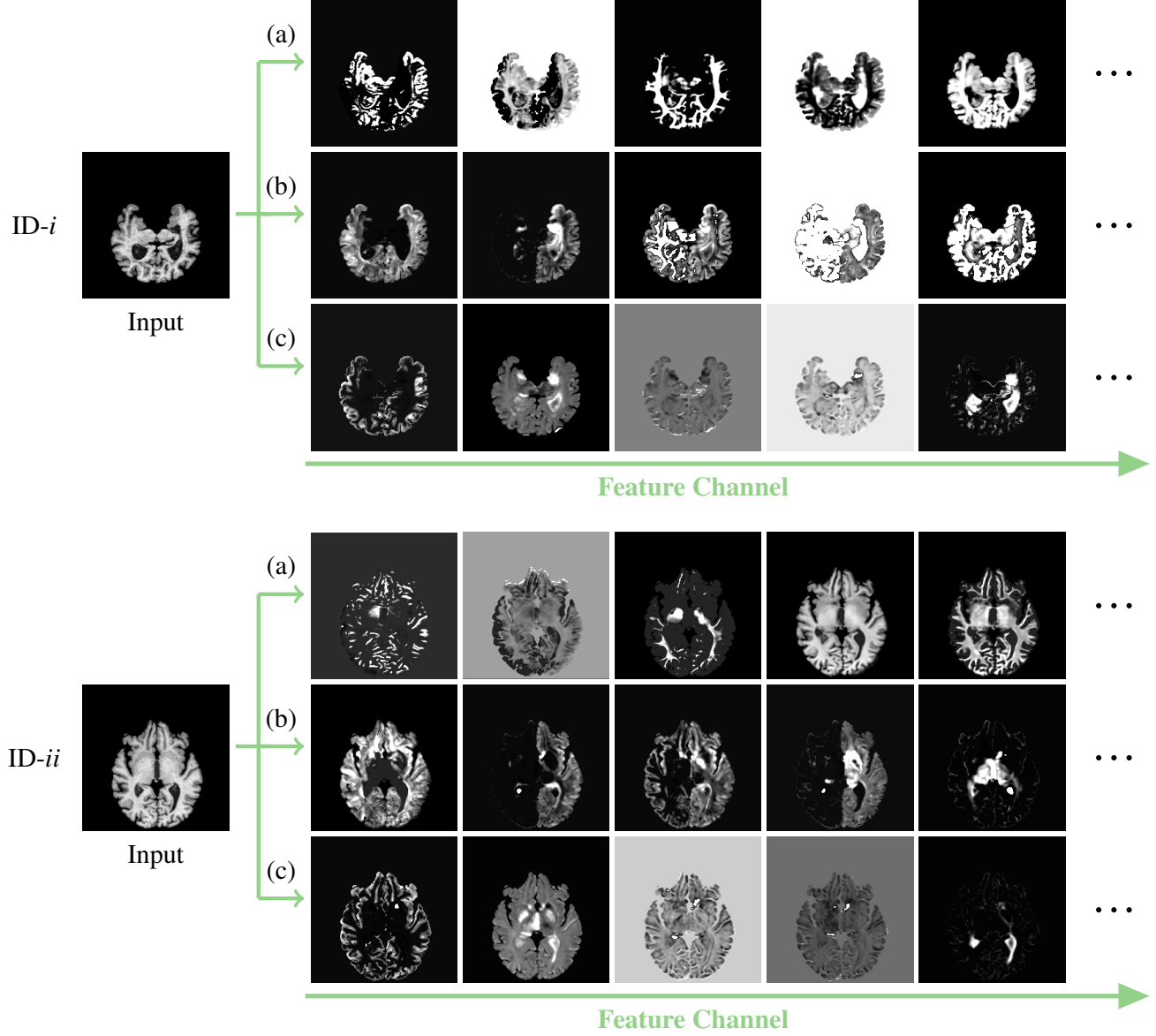


Figure C.1. Visualization comparisons for features computed from (a) Brain-ID (MP-RAGE guided) with its variants: (b) segmentation guided and (c) segmentation + MP-RAGE guided feature representation models. Note that although the two testing subjects here for the three models are the same, their respective selected feature channels are different, for the purpose of better showing different frequency levels of features from each model.

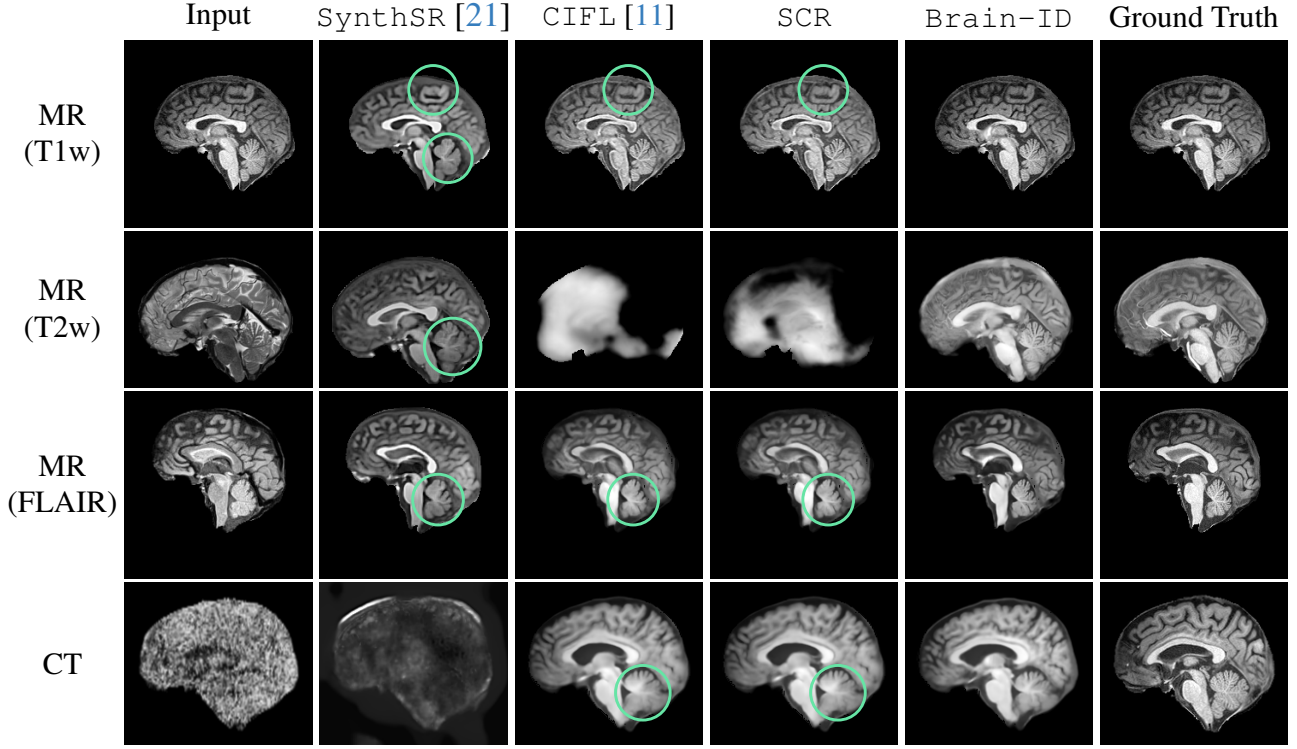


Figure E.2. Qualitative comparisons on the downstream task of anatomy reconstruction/contrast synthesis, between Brain-ID, the baseline SCR, and the state-of-the-art methods CIFL [11], SynthSR [21]. Each row presents the comparison results of inputs with their respective modality/contrast, as indicated in the listing. The green circles highlight some less noticeable details.

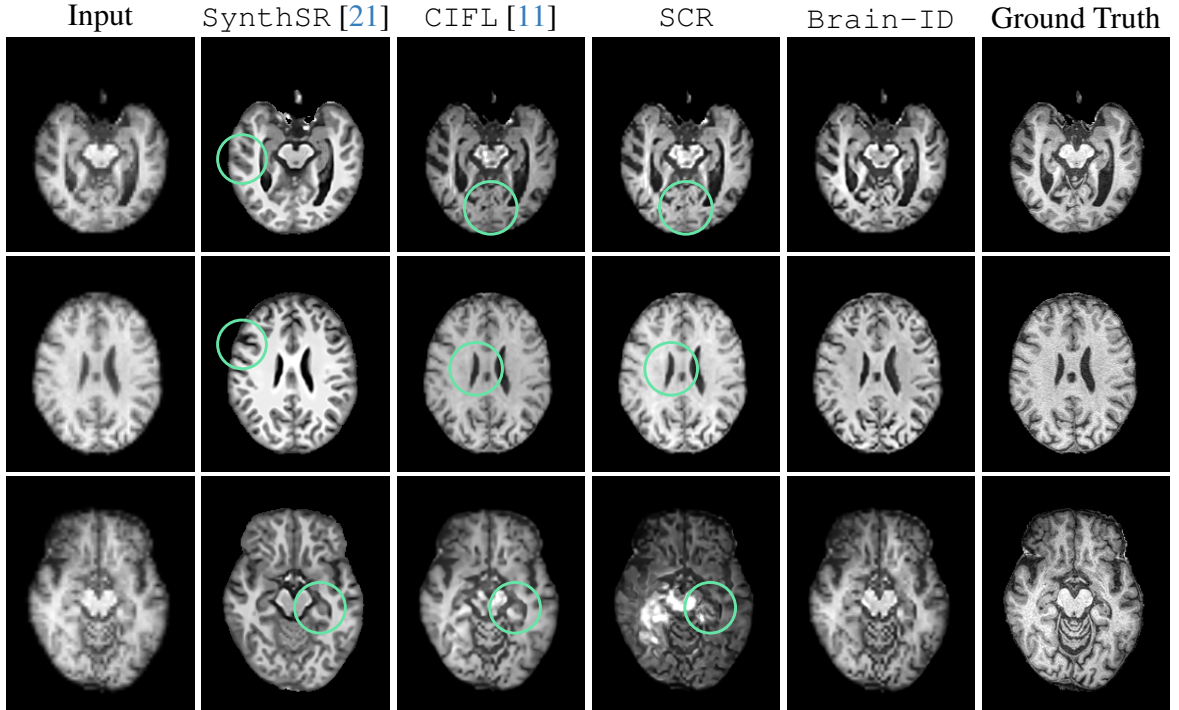


Figure E.3. Qualitative comparisons on the downstream task of image super-resolution, between Brain-ID, the baseline SCR, and the state-of-the-art methods CIFL [11], SynthSR [21]. Each row corresponds to a different testing subject. The green circles highlight some less noticeable details.

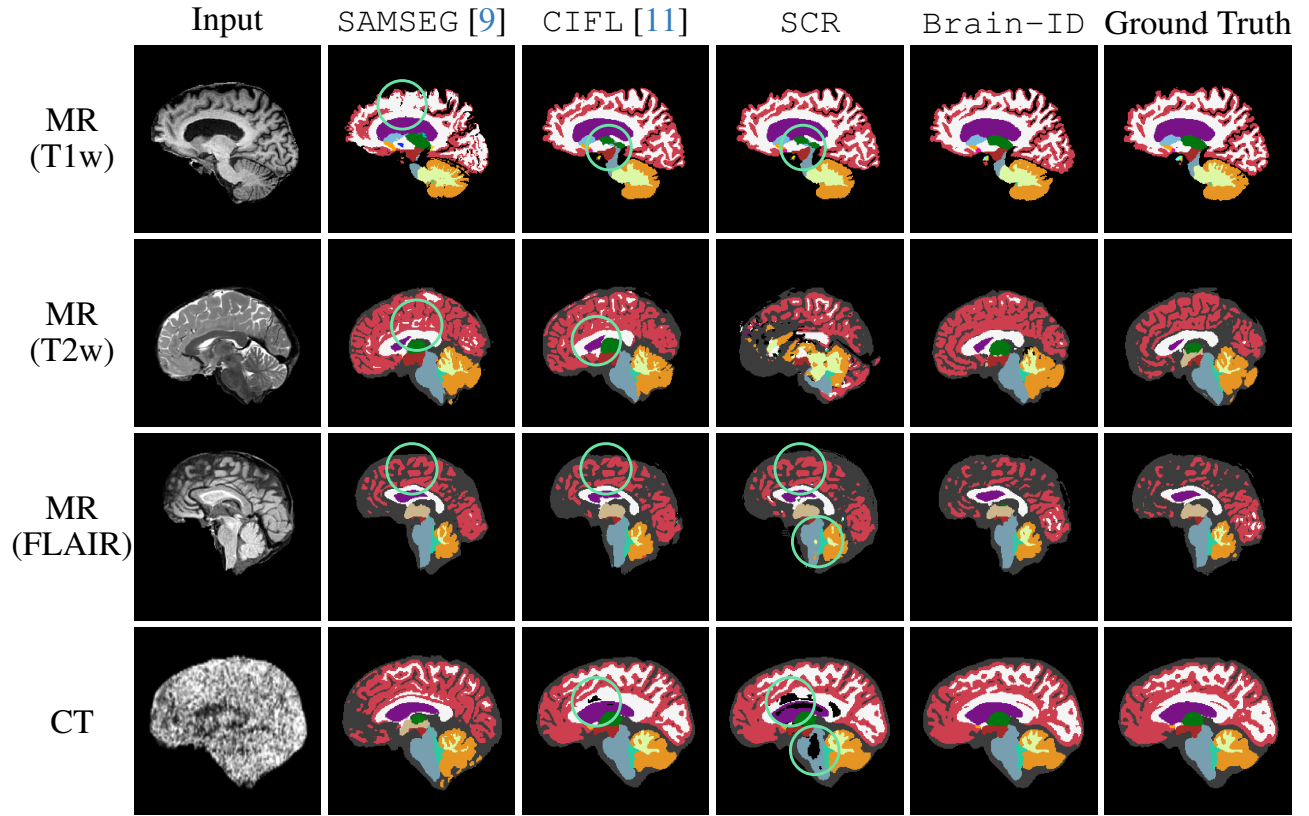


Figure E.4. Qualitative comparisons on the downstream task of brain segmentation, between Brain-ID, the baseline SCR, and the state-of-the-art methods CIFL [11], SAMSEG [9]. Each row presents the comparison results of inputs with their respective modality/contrast, as indicated in the listing. The green circles highlight some less noticeable details.